Two-Dimensional Pattern Formation Modeling with Reaction-Diffusion Equations

Rui Fang, Jiawen Tong

December 18, 2017

1 Introduction

Pattern formation in nature is an intriguing question that has attracted extensive research from biologists and applied mathematicians in the past decades. Originated from Turing's seminal work published in 1952, *The Chemical Basis of Morphogenesis*, reaction-diffusion (RD) equations are the most well-known theoretical models for the mechanism behind self-regulated pattern formation.

Turing's theory proposed a basic idea that spontaneous pattern formation can be sufficiently explained by diffusive and reactive processes of a system of chemical substances. This idea is simple but profound. Over the years, a variety of RD equations have been developed to model patterns in nature, and remarkable similarities between simulation and reality have been observed. For example, Fowler et al. simulated the pigmentation patterns of seashells using the RD equations developed by Meinhardt and Gierer (Figure 1a) [1]. Sanderson et al. produced circular and radial strip-spot patterns found around the eyes of Puffer Fish with RD models modified with radially varied equation parameters (Figure 1b) [2]. Murray used RD models to simulate cats' tails on tapering cylinders with varying width, and successfully recovered the tail patterns of different members of the cat family (Figure 1c) [3].

Most of the RD models having been built and studied, including those used in the three examples above, are two-component models, where only two species of reacting chemicals are considered. According to Meinhardt and Klingler, pattern formation processes generally involve the competition between short-range autocatalytic and long-range inhibitory reactions [4]. This leads to two common two-component RD models, the activator-inhibitor model and the activator-substrate model. Assumed to trigger local pigmentation, the activator chemicals have an autocatalytic (positive) feedback on their own production. The inhibitory process reduces the activator production, either through inhibitor chemicals, which are produced simultaneously with the activator production, or through depletion of substrate chemicals, which are necessary precursors for the activator production [4].

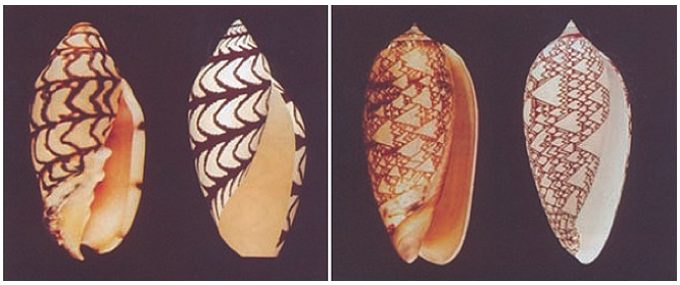

(a) Seashells

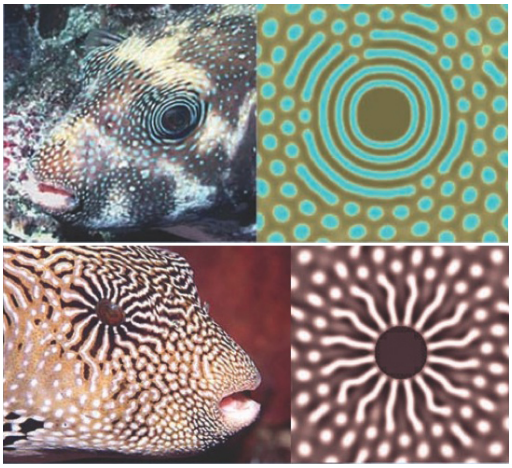

(b) Puffer Fish

(c) Cats

Figure 1: Comparisons between real animal patterns and patterns generated by reaction-diffusion models [1, 2, 3].

There are many possibilities of patterns that can be generated by activator-inhibitor and activator-substrate models. In one-dimensional spatial domain, these models can be used to reproduce lines parallel or perpendicular to the growing edges on seashells [4]. In two-dimensional spatial domain, same equations can yield more complex patterns, such as those seen on the fish skin and mammal coats.

The goal of this project is to study two representative two-dimensional RD models: the Gierer-Meinhardt model (GM, activator-inhibitor) and the Gray-Scott model (GS, activator-substrate) (Section 2). To simulate the pattern formation process with relatively high accuracy and efficiency, we envision to implement four different numerical methods (Section 3) for each model and compare the results and performance of different methods (Section 4). We will also explore the effects of domain, initial conditions, and parameter settings on pattern formation by changing one factor at a time while keeping the others fixed (Section 5).

2 Models

For the interest of studying and comparing the activator-inhibitor and activator-substrate models, we focus on one typical model for each type: the Gierer-Meinhardt Model for the activator-inhibitor type and the Gray-Scott Model for the activator-substrate type.

2.1 Gierer-Meinhardt Model

Proposed by Gierer and Meinhardt in 1972, the following reaction-diffusion equations describe a possible interaction between the autocatalytic activator $u(x, y)$ and its antagonist, the inhibitor $v(x, y)$:

$$\frac{\partial u}{\partial t} = D_u \left(\frac{\partial^2 u}{\partial x^2} + \frac{\partial^2 u}{\partial y^2} \right) + \frac{\rho}{v} \left(\frac{u^2}{1 + \kappa u^2} \right) - \mu_u u + \rho_u \tag{2.1a}$$

$$\frac{\partial v}{\partial t} = D_v \left(\frac{\partial^2 v}{\partial x^2} + \frac{\partial^2 v}{\partial y^2} \right) + \rho \left(\frac{u^2}{1 + \kappa u^2} \right) - \mu_v v \tag{2.1b}$$

where D_u and D_v are the diffusion coefficients, μ_u and μ_v are the decay rates, ρ_u is the basic activator-independent activator production rate, ρ is the source density that describes the cells' ability to perform the non-linear autocatalysis, and $\frac{u^2}{1+\kappa u^2}$ models the saturation of activator production with saturation constant κ.

In this case, the inhibitor v is produced simultaneously with the activator u while the production of u is slowed down by v due to the $1/v$ factor. It is crucial for stable pattern formation that the diffusion of the inhibitor is much faster than that of the activator, i.e., $D_v \gg D_u$ [5].

2.2 Gray-Scott Model

In 1993, Pearson formulated the following reaction-diffusion equations for the simple pattern-forming autocatalytic reactions ($u + 2v \to 3v$, $v \to p$) described by Gray and Scott:

$$\frac{\partial u}{\partial t} = D_u \left(\frac{\partial^2 u}{\partial x^2} + \frac{\partial^2 u}{\partial y^2} \right) - uv^2 + f(1 - u) \tag{2.2a}$$

$$\frac{\partial v}{\partial t} = D_v \left(\frac{\partial^2 v}{\partial x^2} + \frac{\partial^2 v}{\partial y^2} \right) + uv^2 - (k + f)v \tag{2.2b}$$

where D_u and D_v are the diffusion coefficients, f is the feed rate, and k is the kill rate.

In this system, v represents the activator and u represents the substrate (production of v requires u due to the first reaction). The second reaction converts v to an inert product p with the reaction rate k (also called the kill rate). The feed process feeds u and drains u, v and p with the feed rate f [6].

3 Numerical Methods

To numerically solve the above partial differential equations, we discretize u, v as $u^n_{j,k}$, $v^n_{j,k}$ to approximate $u(kh, jh, n\Delta t)$, $v(kh, jh, n\Delta t)$ respectively, where $\Delta x = \Delta y = h$ is the space step size, Δt is the time step size. There are N_x, N_y points in x, y directions, and the domain lengths are $L_x = (N_x - 1)h$, $L_y = (N_y - 1)h$. We implement four numerical methods to solve the equations. All four methods use centered difference scheme in space. One of them is explicit in time and the other three are mixtures of implicit and explicit methods, since the reaction terms are always treated explicitly. Periodic boundary conditions are employed in all methods.

For each method we use, we will briefly discuss the motivation for the method, state its accuracy and stability, and present the discretization formula using the Gray-Scott model (Eq. 2.2) as an example.

3.1 Forward Euler Method

The forward Euler method is a fully explicit method. The solution for each time step is an explicit function of the solution for the last step. Hence the results are fast and straightforward to compute. The forward Euler method is first order accurate in time, and the centered difference scheme applied to the second derivatives is second order accurate in space. Yet, the fully explicit time scheme is subject to numerical instability. The stability analysis of the forward Euler method on the diffusion part shows that a necessary but not sufficient condition for numerical stability is $\Delta t \leq \frac{h^2}{4\max(D_u, D_v)}$.

- Discretization for Gray-Scott Model

$$\begin{aligned}\frac{u^{n+1}_{j,k} - u^n_{j,k}}{\Delta t} = \frac{D_u}{h^2}\left(u^n_{j,k-1} + u^n_{j,k+1} + u^n_{j-1,k} + u^n_{j+1,k} - 4u^n_{j,k}\right) \\ - u^n_{j,k}\left(v^n_{j,k}\right)^2 + f(1 - u^n_{j,k})\end{aligned} \tag{3.1a}$$

$$\begin{aligned}\frac{v^{n+1}_{j,k} - v^n_{j,k}}{\Delta t} = \frac{D_v}{h^2}\left(v^n_{j,k-1} + v^n_{j,k+1} + v^n_{j-1,k} + v^n_{j+1,k} - 4v^n_{j,k}\right) \\ + u^n_{j,k}\left(v^n_{j,k}\right)^2 - (k + f)v^n_{j,k}\end{aligned} \tag{3.1b}$$

- Stability analysis

  Consider the diffusion equation for u:

$$\frac{u^{n+1}_{j,k} - u^n_{j,k}}{\Delta t} = \frac{D_u}{h^2}\left(u^n_{j,k-1} + u^n_{j,k+1} + u^n_{j-1,k} + u^n_{j+1,k} - 4u^n_{j,k}\right). \tag{3.2}$$

Set $u^n_{j,k}(l,m) = \lambda(l,m)^n e^{il(jh)} e^{im(kh)}$. Plug into the equation and simplify, we obtain

$$\frac{\lambda(l,m)^{n+1}}{\lambda(l,m)^n} = 1 - \frac{4D_u\Delta t}{h^2}\left(\sin^2\left(\frac{mh}{2}\right) + \sin^2\left(\frac{lh}{2}\right)\right). \tag{3.3}$$

We wish to find conditions for which $|\lambda(l,m)| \leq 1$. Here, $\lambda(l,m)$ cannot be greater than 1. Thus we want

$$1 - \frac{4D_u\Delta t}{h^2}\left(\sin^2\left(\frac{mh}{2}\right) + \sin^2\left(\frac{lh}{2}\right)\right) \geq -1. \tag{3.4}$$

Since the $\sin^2$ terms can at most go up to 1,

$$\Delta t \leq \frac{h^2}{4D_u}. \tag{3.5}$$

When we solve for u and v concurrently, the actual time step constraint is

$$\Delta t \leq \frac{h^2}{4\max(D_u, D_v)}. \tag{3.6}$$

3.2 Backward Euler Method

To alleviate the time step size constraint induced by the explicit diffusion part, we implement the implicit backward Euler Method for the diffusion terms while keeping other terms explicit. This would still give us first order accuracy in time, and second order accuracy in space. Although the time step size is allowed to be larger now, solving the equations at each time step involves solving $N = N_x \times N_y$ linear equations (the corresponding matrix $A \in \mathbb{R}^{N\times N}$), which is very computationally expensive compared to fully explicit method.

- Discretization for Gray-Scott Model

$$\begin{aligned}\frac{u^{n+1}_{j,k} - u^n_{j,k}}{\Delta t} = \frac{D_u}{h^2}\left(u^{n+1}_{j,k-1} + u^{n+1}_{j,k+1} + u^{n+1}_{j-1,k} + u^{n+1}_{j+1,k} - 4u^{n+1}_{j,k}\right) \\ - u^n_{j,k}\left(v^n_{j,k}\right)^2 + f(1 - u^n_{j,k})\end{aligned} \tag{3.7a}$$

$$\begin{aligned}\frac{v^{n+1}_{j,k} - v^n_{j,k}}{\Delta t} = \frac{D_v}{h^2}\left(v^{n+1}_{j,k-1} + v^{n+1}_{j,k+1} + v^{n+1}_{j-1,k} + v^{n+1}_{j+1,k} - 4v^{n+1}_{j,k}\right) \\ + u^n_{j,k}\left(v^n_{j,k}\right)^2 - (k+f)v^n_{j,k}\end{aligned} \tag{3.7b}$$

3.3 Crank-Nicolson Method

Alternatively, we implement the implicit Crank-Nicolson method for the diffusion part to reduce the time step size constraint. The advantage of using Crank-Nicolson method over backward Euler method is the improved accuracy in time. Crank-Nicolson method is a second order accurate method. Therefore the order of accuracy for the mixture of Crank-Nicolson method and fully explicit method is expected to be somewhere between one and two. The computational cost of this method is, however, still very big.

- Discretization for Gray-Scott Model

$$\begin{aligned}\frac{u_{j,k}^{n+1}-u_{j,k}^{n}}{\Delta t} &= \frac{D_u}{2h^2}\left(u_{j,k-1}^{n}+u_{j,k+1}^{n}+u_{j-1,k}^{n}+u_{j+1,k}^{n}-4u_{j,k}^{n}\right)\\ &+\frac{D_u}{2h^2}\left(u_{j,k-1}^{n+1}+u_{j,k+1}^{n+1}+u_{j-1,k}^{n+1}+u_{j+1,k}^{n+1}-4u_{j,k}^{n+1}\right)\\ &-u_{j,k}^{n}\left(v_{j,k}^{n}\right)^2+f(1-u_{j,k}^{n})\end{aligned} \tag{3.8a}$$

$$\begin{aligned}\frac{v_{j,k}^{n+1}-v_{j,k}^{n}}{\Delta t} &= \frac{D_v}{2h^2}\left(v_{j,k-1}^{n}+v_{j,k+1}^{n}+v_{j-1,k}^{n}+v_{j+1,k}^{n}-4v_{j,k}^{n}\right)\\ &+\frac{D_v}{2h^2}\left(v_{j,k-1}^{n+1}+v_{j,k+1}^{n+1}+v_{j-1,k}^{n+1}+v_{j+1,k}^{n+1}-4v_{j,k}^{n+1}\right)\\ &+u_{j,k}^{n}\left(v_{j,k}^{n}\right)^2-(k+f)v_{j,k}^{n}\end{aligned} \tag{3.8b}$$

3.4 Alternating Direction Implicit (ADI) Method

The ADI method is an example of operator splitting method, and it is implemented for the diffusion terms to significantly reduce the computational work required for the backward Euler and Crank-Nicolson methods. The idea behind the ADI method is to treat the x-derivative and y-derivative separately in order to alternately solve along the x-direction and y-direction. For example, by splitting each time step into two stages, we first take the x-derivative implicitly and y-derivative explicitly, and then take the x-derivative explicitly and y-derivative implicitly. This way, the involved matrices are small in size ($A \in \mathbb{R}^{N_x \times N_x}$ or $A \in \mathbb{R}^{N_y \times N_y}$) and much easier to solve because they are tridiagonal. It can be shown that the ADI method is second order in time and space [7]. A stability analysis shows that the ADI method is unconditionally stable when implemented for the diffusion terms. Therefore, the constraint on the time step comes from explicit reaction terms only, and is expected to be small.

- Discretization for Gray-Scott Model

Stage 1: solve along x-direction

$$\frac{u_{j,k}^{n+\frac{1}{2}} - u_{j,k}^{n}}{\Delta t/2} = \frac{D_u}{h^2}\left[\left(u_{j,k-1}^{n+\frac{1}{2}} - 2u_{j,k}^{n+\frac{1}{2}} + u_{j,k+1}^{n+\frac{1}{2}}\right) + \left(u_{j-1,k}^{n} - 2u_{j,k}^{n} + u_{j+1,k}^{n}\right)\right] - u_{j,k}^{n}\left(v_{j,k}^{n}\right)^2 + f(1 - u_{j,k}^{n}) \tag{3.9a}$$

$$\frac{v_{j,k}^{n+\frac{1}{2}} - v_{j,k}^{n}}{\Delta t} = \frac{D_v}{h^2}\left[\left(v_{j,k-1}^{n+\frac{1}{2}} - 2v_{j,k}^{n+\frac{1}{2}} + v_{j,k+1}^{n+\frac{1}{2}}\right) + \left(v_{j-1,k}^{n} - 2v_{j,k}^{n} + v_{j+1,k}^{n}\right)\right] + u_{j,k}^{n}\left(v_{j,k}^{n}\right)^2 - (k+f)v_{j,k}^{n} \tag{3.9b}$$

Stage 2: solve along y-direction

$$\frac{u_{j,k}^{n+1} - u_{j,k}^{n+\frac{1}{2}}}{\Delta t/2} = \frac{D_u}{h^2}\left[\left(u_{j,k-1}^{n+\frac{1}{2}} - 2u_{j,k}^{n+\frac{1}{2}} + u_{j,k+1}^{n+\frac{1}{2}}\right) + \left(u_{j-1,k}^{n+1} - 2u_{j,k}^{n+1} + u_{j+1,k}^{n+1}\right)\right] - u_{j,k}^{n+\frac{1}{2}}\left(v_{j,k}^{n+\frac{1}{2}}\right)^2 + f(1 - u_{j,k}^{n+\frac{1}{2}}) \tag{3.10a}$$

$$\frac{v_{j,k}^{n+1} - v_{j,k}^{n+\frac{1}{2}}}{\Delta t} = \frac{D_v}{h^2}\left[\left(v_{j,k-1}^{n+\frac{1}{2}} - 2v_{j,k}^{n+\frac{1}{2}} + v_{j,k+1}^{n+\frac{1}{2}}\right) + \left(v_{j-1,k}^{n+1} - 2v_{j,k}^{n+1} + v_{j+1,k}^{n+1}\right)\right] + u_{j,k}^{n+\frac{1}{2}}\left(v_{j,k}^{n+\frac{1}{2}}\right)^2 - (k+f)v_{j,k}^{n+\frac{1}{2}} \tag{3.10b}$$

- Stability analysis

  Apply ADI method to the diffusion equation:

$$\frac{u_{j,k}^{n+\frac{1}{2}} - u_{j,k}^{n}}{\Delta t/2} = \frac{D_u}{h^2}\left[\left(u_{j,k-1}^{n+\frac{1}{2}} - 2u_{j,k}^{n+\frac{1}{2}} + u_{j,k+1}^{n+\frac{1}{2}}\right) + \left(u_{j-1,k}^{n} - 2u_{j,k}^{n} + u_{j+1,k}^{n}\right)\right] \tag{3.11}$$

$$\frac{u_{j,k}^{n+1} - u_{j,k}^{n+\frac{1}{2}}}{\Delta t/2} = \frac{D_u}{h^2}\left[\left(u_{j,k-1}^{n+\frac{1}{2}} - 2u_{j,k}^{n+\frac{1}{2}} + u_{j,k+1}^{n+\frac{1}{2}}\right) + \left(u_{j-1,k}^{n+1} - 2u_{j,k}^{n+1} + u_{j+1,k}^{n+1}\right)\right] \tag{3.12}$$

Set $u_{j,k}^n(l,m) = \lambda(l,m)^n e^{il(jh)} e^{im(kh)}$. Plug into the equations and simplify, we obtain

$$\frac{\lambda(l,m)^{n+\frac{1}{2}}}{\lambda(l,m)^n} = \frac{1 - \frac{2D_u\Delta t}{h^2}\sin^2\left(\frac{lh}{2}\right)}{1 + \frac{2D_u\Delta t}{h^2}\sin^2\left(\frac{mh}{2}\right)}, \tag{3.13}$$

$$\frac{\lambda(l,m)^{n+1}}{\lambda(l,m)^{n+\frac{1}{2}}} = \frac{1 - \frac{2D_u\Delta t}{h^2}\sin^2\left(\frac{mh}{2}\right)}{1 + \frac{2D_u\Delta t}{h^2}\sin^2\left(\frac{lh}{2}\right)}. \tag{3.14}$$

Combine together,

$$\frac{\lambda(l,m)^{n+1}}{\lambda(l,m)^n} = \frac{1 - \frac{2D_u\Delta t}{h^2}\sin^2\left(\frac{lh}{2}\right)}{1 + \frac{2D_u\Delta t}{h^2}\sin^2\left(\frac{mh}{2}\right)} \cdot \frac{1 - \frac{2D_u\Delta t}{h^2}\sin^2\left(\frac{mh}{2}\right)}{1 + \frac{2D_u\Delta t}{h^2}\sin^2\left(\frac{lh}{2}\right)}. \tag{3.15}$$

Let $\alpha = \frac{2D_u\Delta t}{h^2}\sin^2\left(\frac{lh}{2}\right)$, $\beta = \frac{2D_u\Delta t}{h^2}\sin^2\left(\frac{mh}{2}\right)$, then

$$\lambda(l,m) = \frac{(1-\alpha)(1-\beta)}{(1+\beta)(1+\alpha)}. \tag{3.16}$$

Because $\alpha \geq 0$ and $\beta \geq 0$, $-1 < \frac{1-\alpha}{1+\alpha} \leq 1$ and $-1 < \frac{1-\beta}{1+\beta} \leq 1$. Therefore, $|\lambda(l,m)| \leq 1$. The ADI method is unconditionally stable.

4 Experiments and Results

We implemented four numerical methods to compute the solution for the Gierer-Meinhardt (GM) model and the Gray-Scott (GS) model. For each method, we 1) computed the evolution of the pattern over time and visualized them using 2D contour plot, 2) saved the evolution of the pattern matrix's mean deducted Frobenius norm to gain an intuitive sense of the onset time of a stable pattern, and 3) recorded the runtime of each method.

In all the contour plots, red represents large values, blue represent small values, and white is in between. The levels of each 2D pattern's contour plot are determined by the maximum and minimum value of the pattern matrix. Thus, the differences of color across plots may not imply differences in values.

4.1 Gierer-Meinhardt Model

4.1.1 Pattern Formation

In all implementations, we used grid setting $N_x = 40$, $N_y = 40$, $h = 2$; parameters $D_u = 0.02$, $D_v = 2$, $\rho = 0.001$, $\rho_u = 0.001$, $\mu_u = 0.02$, $\mu_v = 0.03$, $\kappa = 0.1$; initial conditions $v^0_{j,k} = 0.1$ and $u^0_{j,k}$ are randomly drawn from a normal distribution with mean=0.5 and std=0.1. For forward Euler method, $\Delta t = 0.25$; for backward Euler, Crank-Nicolson and ADI methods, $\Delta t = 20$. The end simulation time is 10000(s).

As shown in Figure 2,3,4,5, the evolution of patterns and their ending states look similar among different methods, while their mean deducted Frobenius norm changed differently over time. The norm firstly grows and peaks before t=200(s). For each method, the norm slowed down its growth after t=1000(s) and reached a stable state after t=2500(s). Thus, we also plotted the evolution of the patterns before t=1000(s) and t=2500(s) to gain a more detailed sense of the pattern's formation process.[1]

4.1.2 Numerical Stability and Runtime Analysis

The explicit forward Euler method is expected to have the smallest limit for time step size ($\Delta t \leq \frac{h^2}{4\max(D_u, D_v)}$), while the other 3 partially implicit (implicit for diffusion term and explicit for reaction terms) methods are expected to have larger limit for Δt. We numerically checked the limit of Δt for each method. The results are summarized in Table 1. In general the results matched our expectation. The explicit forward Euler method has the most rigorous limit ($max(\Delta t) = 0.45$), the other three implicit methods allow Δt to be much larger ($max(\Delta t) > 40$).

Since we used much larger Δt in implicit methods than in the Forward Euler method, the runtimes of implicit methods are much shorter than that of Forward Euler. We expect the runtime of the ADI method to be the shortest among all implicit methods since it solves

[1]Complete results are included in the website https://jasmineeeeetong.github.io/AM205_17Fall_Project_Publish/

a smaller matrix of tridiagonal form. But as we did not use a fast enough solver (i.e, the tridiagonal matrix algorithm) and the size of the grid (40×40) is not too large, the actual runtime of the ADI method is longer than that of the other implicit methods.

Method	Runtime	Stability limit for Δt
Forward Euler	11.244	0.45
Backward Euler	0.736	42
Crank Nicolson	0.828	44
ADI method	0.957	64

Table 1: GM: Runtime and Stability limit for Δt

4.2 Gray-Scott Model

4.2.1 Pattern Formation

In all implementations, we used grid setting $N_x = 64$, $N_y = 64$, $h = 2$; parameters $D_u = 1.0$, $D_v = 0.5$, $f = 0.055$, $k = 0.062$; initial conditions $u^0_{j,k} = 1$ for all j, k, $v^0_{j,k} = 1$ if $24 \leq j \leq 39, 24 \leq k \leq 39$ and 0 elsewhere. For forward Euler method, $\Delta t = 0.5$; for backward Euler and Crank-Nicolson methods, $\Delta t = 1$; for ADI methods, $\Delta t = 1.5$. The end simulation time is 10000(s).

As shown in Figure 6,7,8,9, the patterns' evolution over time and ending states solved by forward Euler, backward Euler and Crank-Nicolson method are similar but different from the results given by the ADI method. Such discrepancies still appear after we adjusted grid spacings. This suggests that there might be something intrinsic to the ADI method that caused the difference. In addition, the behaviors of the explicit nonlinear reaction terms are not fully understood, therefore could be a source of unexpected results.

Judging from the evolution of the mean deducted Frobenius norm of the U and V matrices, the norm firstly grows and peaks before t=10(s). The norm entered a stable phase after t=100(s) and almost stayed the same after t=2000(s). Thus, we also plotted the evolution of the patterns before t=100(s) and t=2000(s) to gain a more detailed sense of the pattern's formation process.[2]

4.2.2 Numerical Stability and Runtime Analysis

The explicit forward Euler method is expected to have the smallest limit for time step size ($\Delta t \leq \frac{h^2}{4\max(D_u, D_v)}$), while the other 3 partially implicit (implicit for diffusion term and explicit for reaction terms) methods are expected to have larger limit for dt. We numerically checked the limit of time step size (Δt) for each method. The results are summarized in Table 2. The results matched our expectation. Similar to the GM model,

[2]Complete results are included in the website https://jasmineeeeetong.github.io/AM205_17Fall_Project_Publish/

the explicit forward Euler method has the most rigorous limit ($max(\Delta t) = 0.9$), the other three implicit methods allow Δt to be larger ($max(\Delta t) \leq 1.3$).

As we used comparable time step size ($\Delta t \sim 1$) among all methods, the runtimes of the explicit Forward Euler is shorter than any other implicit method. We expect the runtime of the ADI method to be the shortest among all implicit methods since it solves a smaller matrix of tridiagonal form and since we used the largest Δt for the ADI method ($\Delta t = 1.5$). The actual runtimes matched our expectation.

Method	Runtime	Stability limit for Δt
Forward Euler	8.467	0.9
Backward Euler	41.290	1.3
Crank Nicolson	40.756	1.3
ADI method	11.599	1.7

Table 2: GS: Runtime and Stability limit for Δt

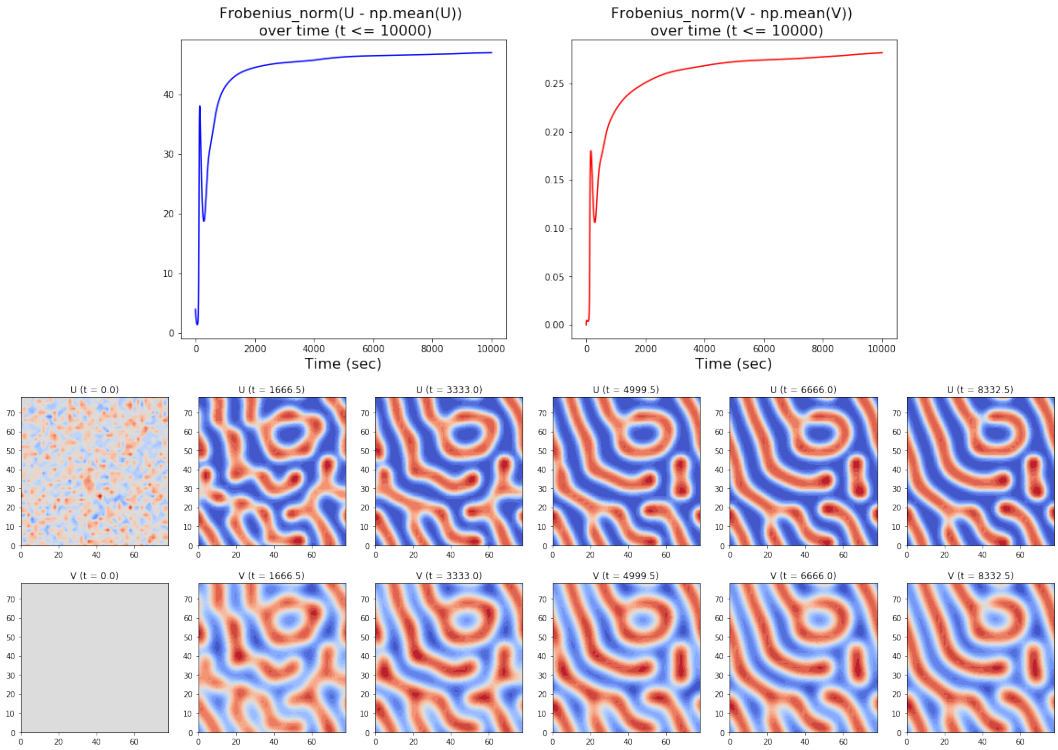

Figure 2: GM: Forward Euler Results

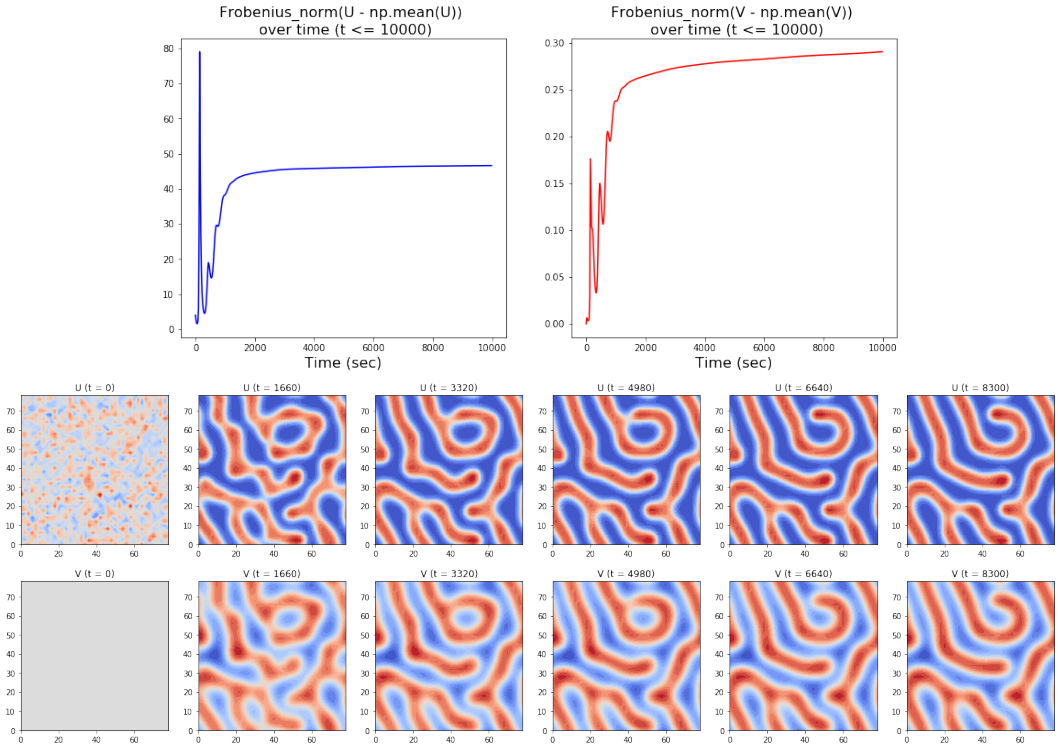

Figure 3: GM: Backward Euler Results

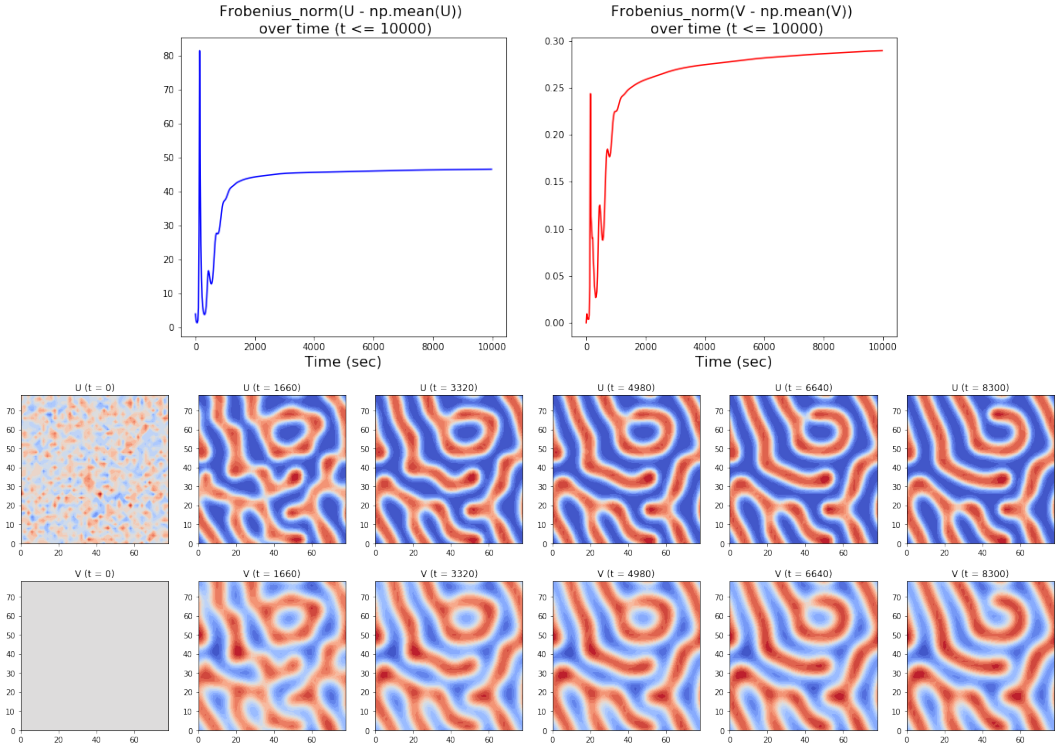

Figure 4: GM: Crank-Nicolson Results

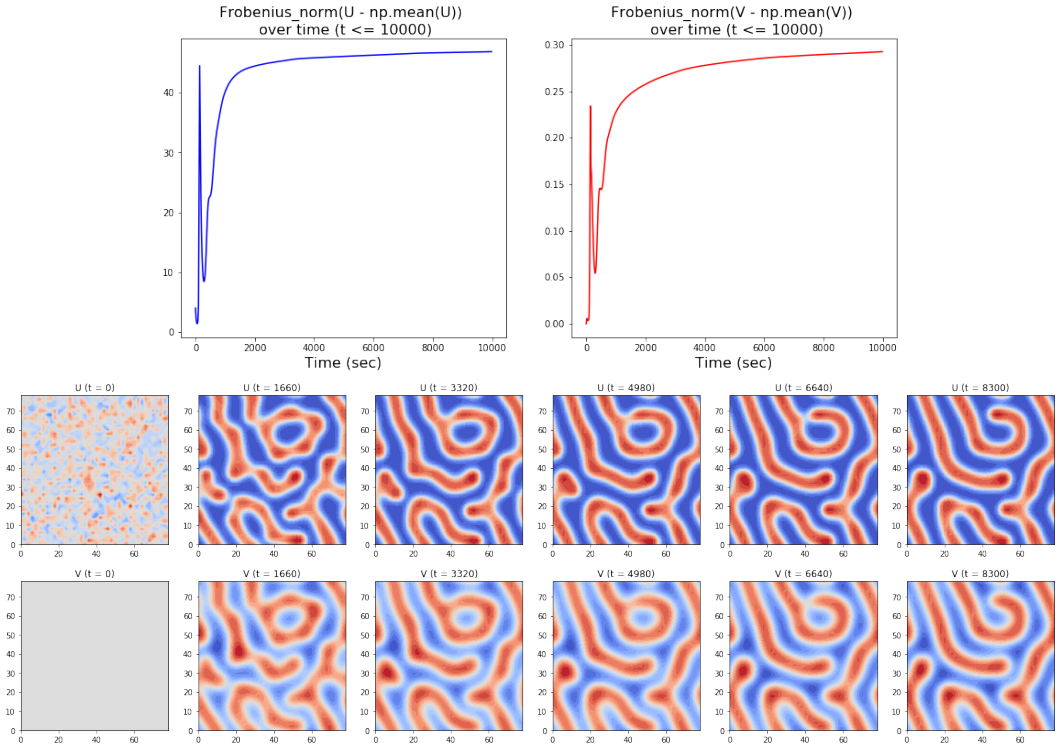

Figure 5: GM: ADI Results

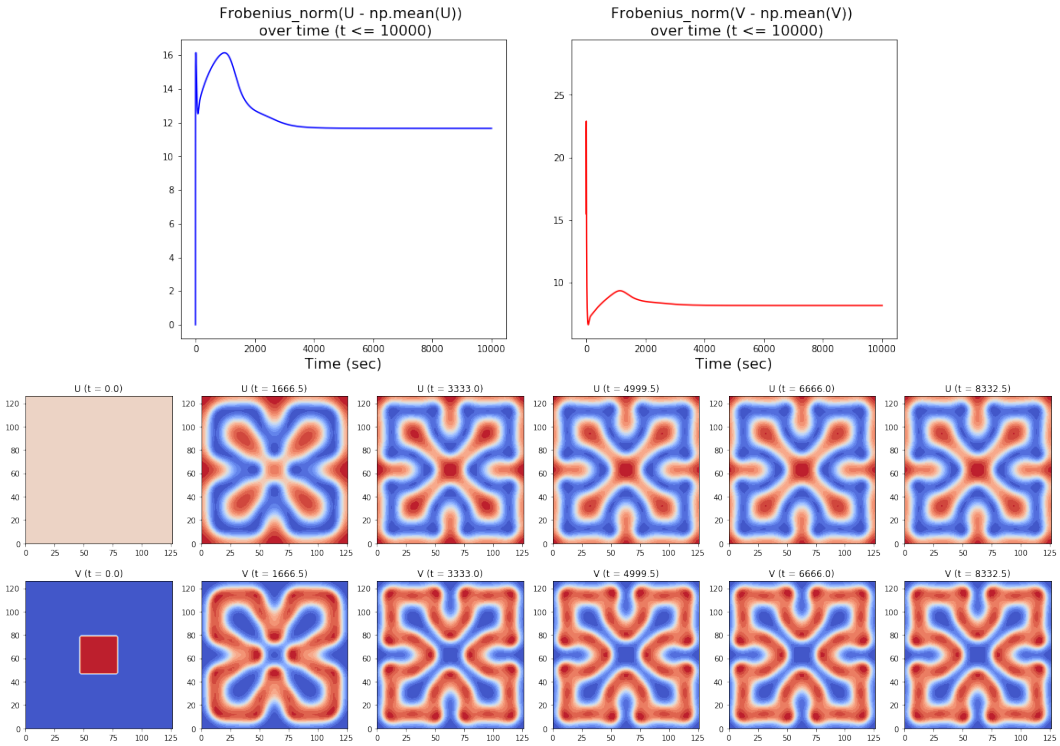

Figure 6: GS: Forward Euler Results

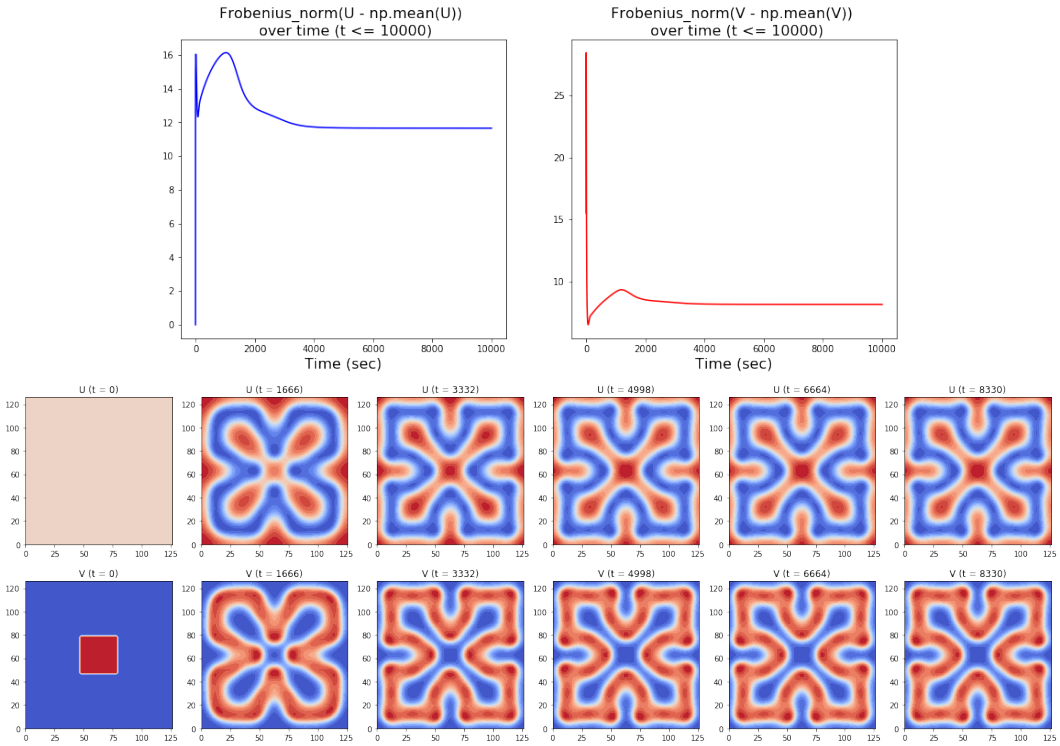

Figure 7: GS: Backward Euler Results

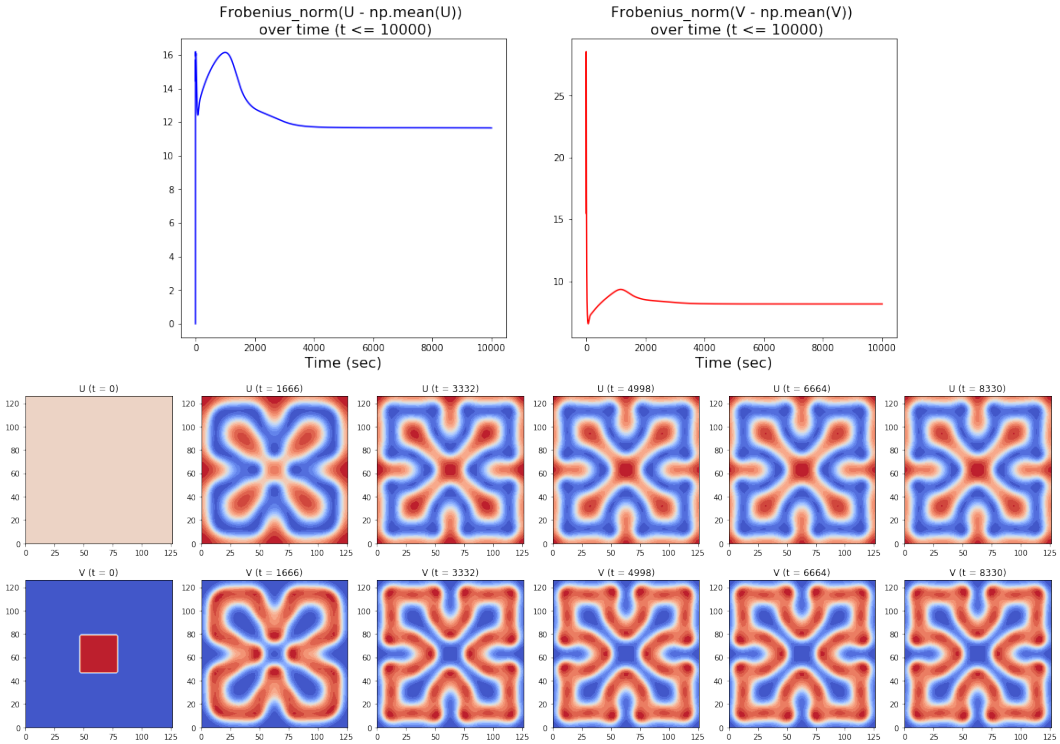

Figure 8: GS: Crank-Nicolson Results

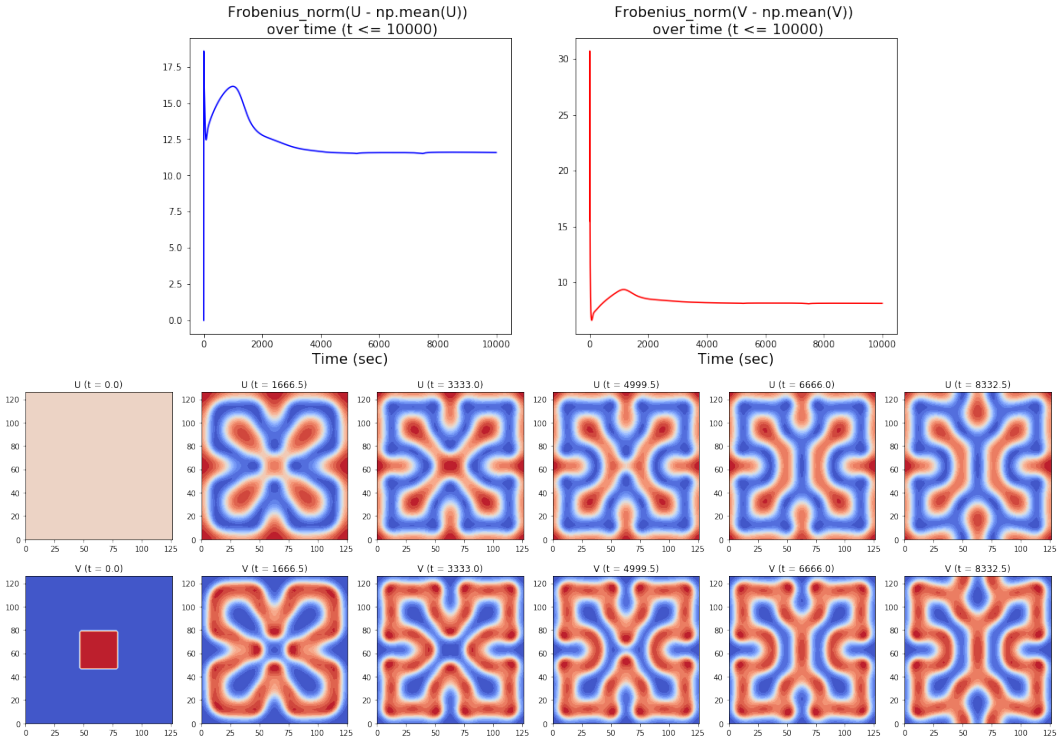

Figure 9: GS: ADI Results

5 Effects of Domain, Initial Conditions and Parameters

To study the effect of domain, initial conditions and each specific parameter in the model, we changed one of those factors at a time while kept the others fixed. We chose to use ADI method to compute the solutions for the RD equations in this section since it is comparatively the most accurate and the most stable (allows the largest Δt) among all the 4 methods we tried.

5.1 Effects of Domain

Shown in Figure 10, as we increased the y-direction domain, we saw the following types of patterns modeled by the GM model's activator component (u): 1) vertical stripes against the x-direction, 2) approximately parallel stripes against the x-direction, 3) a combination of spots and short-length stripes, and 4) more complicated combination of spots and stripes.

Shown in Figure 11, as we increased the y-direction domain, we saw the following types of patterns modeled by the GS model's activator component (v): 1) vertical stripes against the x-direction, 2) parallel stripes to the x-direction, 3) simple rectangular patterns, and 4) more complicated rectangular patterns.

The results of changing the domain corresponds to Murray's claim on the pattern of animal tails that narrow domains allow only bands to grow while large domains allow spots or more complicated pattern to form [3].

5.2 Effects of Initial Conditions

For both the GM and the GS model, different initial conditions will generate different patterns. The ending state patterns preserved the symmetry of the initial conditions.

Shown in Figure 12, in the GM model, on the square domain, the initial condition of random numbers formed random spots or stripes.The centered clusters of 1's formed a set of square boundaries with different side lengths and the same symmetry of the initial cluster. The two clusters of 1's formed an irregular pattern with the same symmetry of the initial two clusters.

Shown in Figure 13, in the GS model, the initial condition of centered cluster of 1's formed a central point symmetric rectangular pattern. The two square clusters of 1's formed a square-like pattern with the same symmetry of the initial two clusters. The two random clusters of 1's formed an irregular pattern with the same symmetry of the initial two clusters. The centered band of 1's formed a series of bands parallel to the initial band.

5.3 Effects of Parameters

In order to generate a stable pattern, each parameter in the GM or GS model should stay within its range. See the results of changing parameters of the GM model in Figure 14, results of changing parameters of the GS model in Figure 15.

5.3.1 Effects of Parameters in the GM model

- Diffusion rates

  When $D_v = 2$, $D_u \sim (0.006, 0.090)$; when $D_u = 0.02$, $D_v > 0.28$.

  The diffusion rate of the activator (D_u) should be much smaller than the the diffusion rate of the inhibitor (D_v). In this way, we maintained the conditions for short-range autocatalytic process and the long-range inhibitory process.

- Source density

  $\rho \sim (10^{-55}, 10^{80})$

  For stability, the source density cannot be too small or too large. If the source density is too small, the effect of reaction is too small compared to diffusion. Otherwise, if the source density is too large, the effect of diffusion is too small compared to reaction. Since we need to keep both reaction terms and diffusion terms in the pattern formation process, the source density should be within some reasonable range.

- Basic activator production rate

  $\rho_u \sim (0, 0.006)$

  According to Meinhardt's activator-inhibitor system, a small activator production rate can initiate the system at low activator concentrations, which is a requirement for pattern formation. The numerically tested upper range for the activator production rate is 0.006 in our experiment.

- Decay rates of the activator and the inhibitor:

  When $\mu_v = 0.03$, $\mu_u \sim (0.015, 0.040)$; when $\mu_u = 0.02$, $\mu_v \sim (0.012, 0.047)$.

  According to Meinhardt's activator-inhibitor system, in order to generate a stable pattern, the decay rate of the inhibitor should be larger than the decay rate of the activator ($\mu_v > \mu_u$). Based on our experiments, the difference between the two decay rates cannot be too large. If the condition that $\mu_v > \mu_u$ is satisfied, the pattern will be stripes. Otherwise, some pattern can still form, but will be mostly spots.

- Saturation constant

  $\kappa \sim (0.005, 0.26)$

  In general, the saturation constant controls the range of the non-linear reaction terms. To get stable patterns, a large range of the non-linear reaction terms is required. A large saturation constant renders a small range for the non-linear reaction terms, which will prevent stable patterns to form. Based on our experiments, the saturation constant could be very close to zero, but cannot exceed 0.26.

5.3.2 Effects of Parameters in the GS model

- Diffusion rates

  When $D_v = 0.5$, $D_u \sim (0.9, 7.5)$; when $D_u = 1$, $D_v \sim (0.15, 0.55)$.

  The diffusion rate of the activator (D_v) should be much smaller than the the diffusion rate of the substrate (D_u). In this way, we maintained the conditions for short-range autocatalytic process and the long-range inhibitory process.

- Feed rate and kill rate

  When $k = 0.062$, $f \sim (0.030, 0.070)$; when $f = 0.055$, $k \sim (0.061, 0.066)$.

  Referring to Pearson's Parametrization[3], different combination of specific feed rate and kill rate renders different types of patterns. Based on our experiments with initial condition as a centered cluster of ones in the activator component, we got equally spaced spots, square-like patterns, and symmetric stripes at the 4 corners of the square domain.

[3] http://mrob.com/pub/comp/xmorphia/

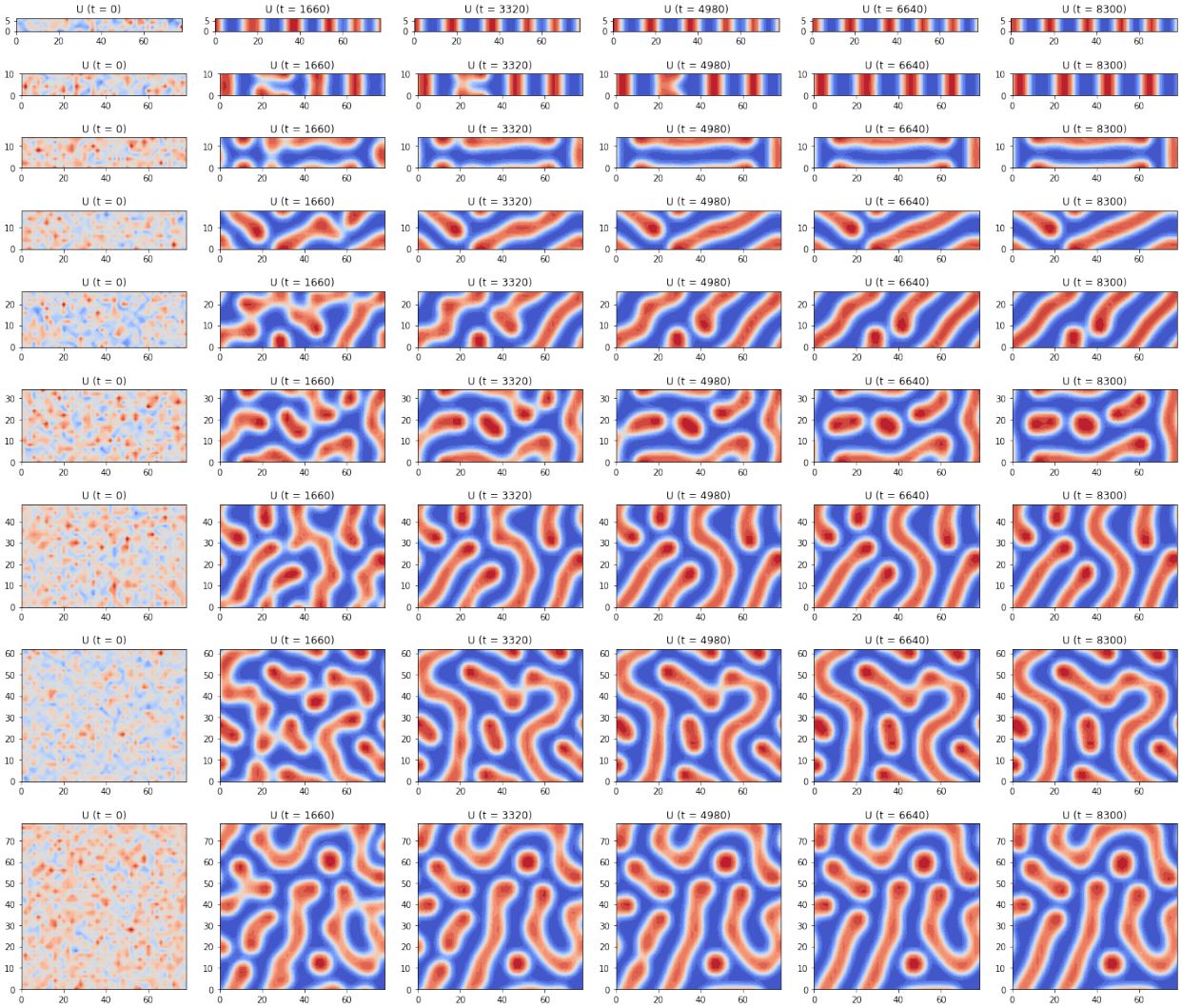

Figure 10: GM: Effects of Domain

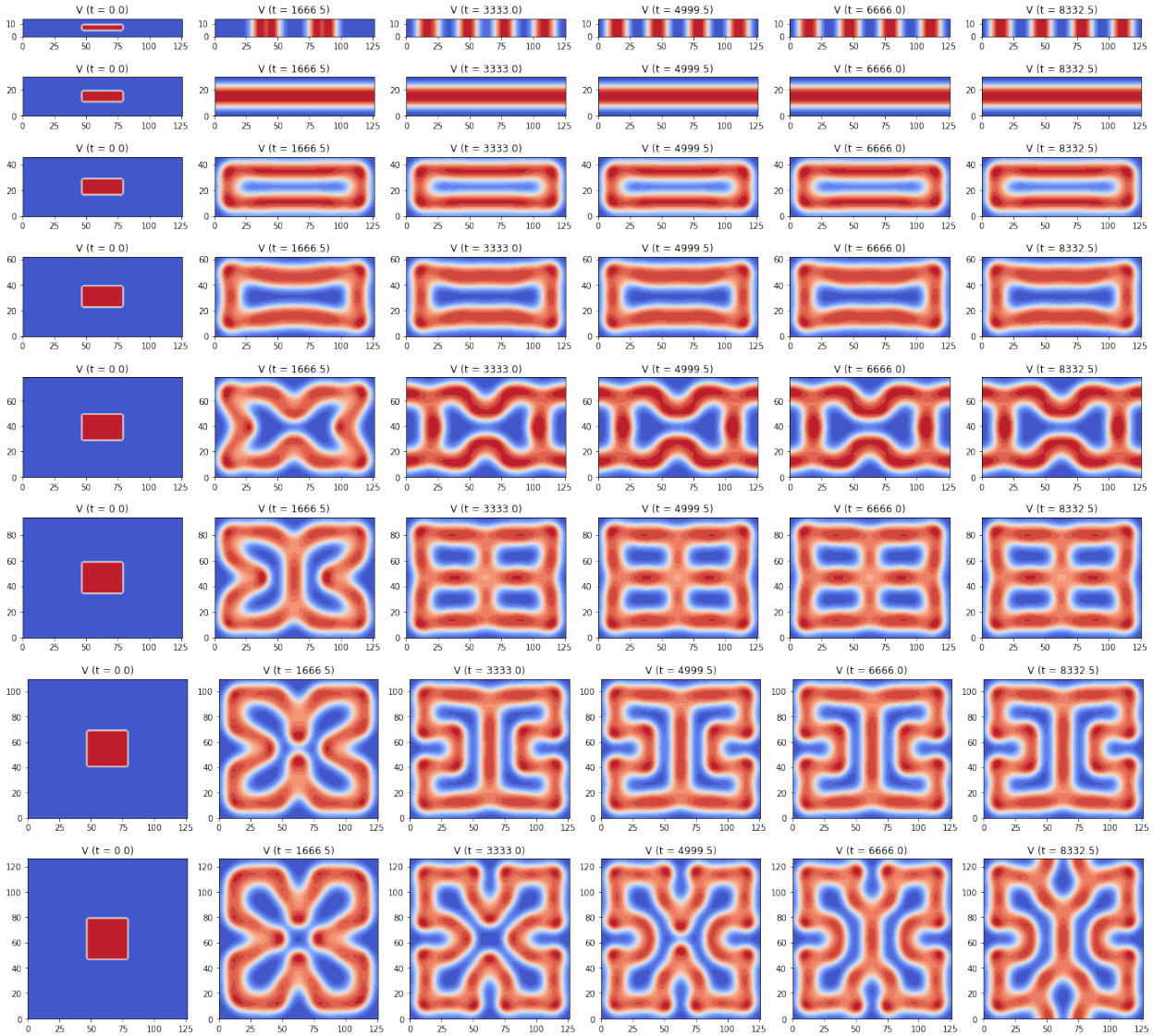

Figure 11: GS: Effects of Domain

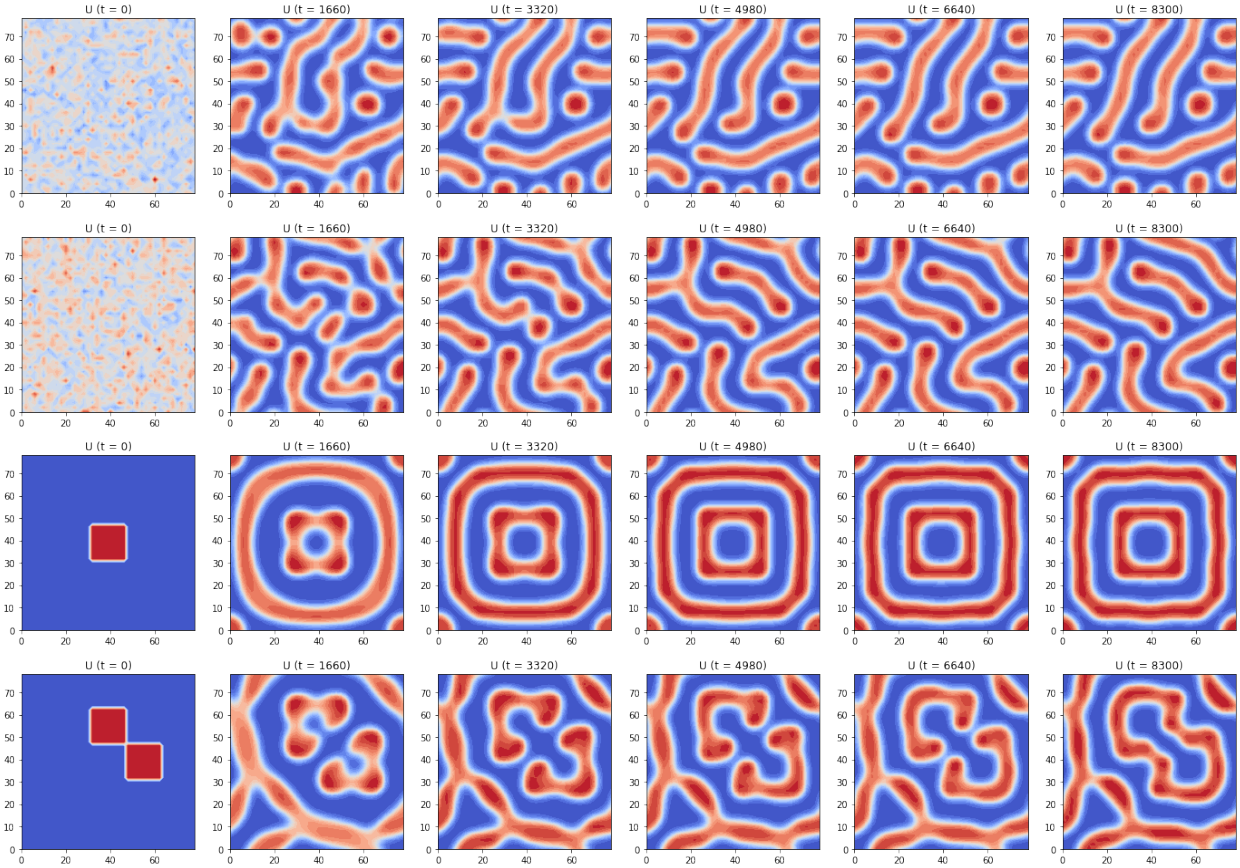

Figure 12: GM: Effects of Initial Conditions

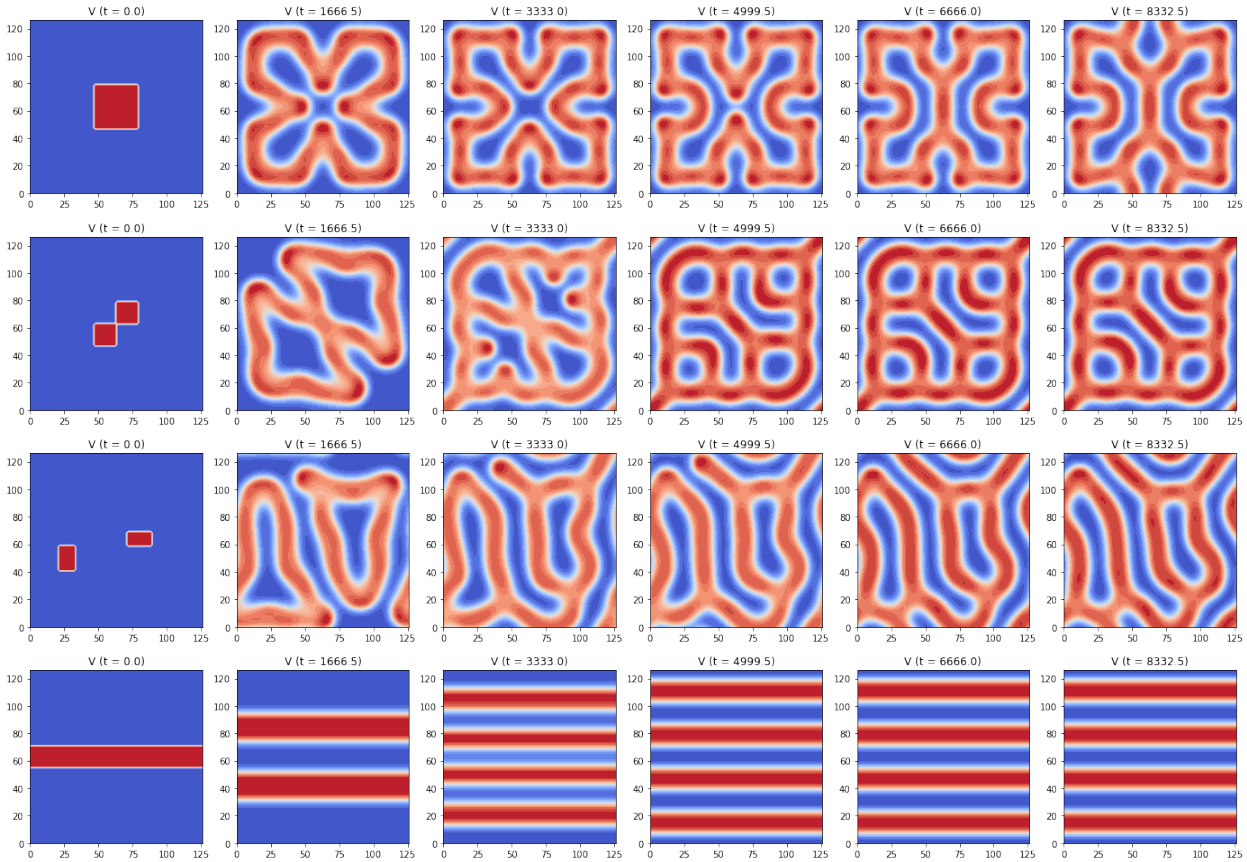

Figure 13: GS: Effects of Initial Conditions

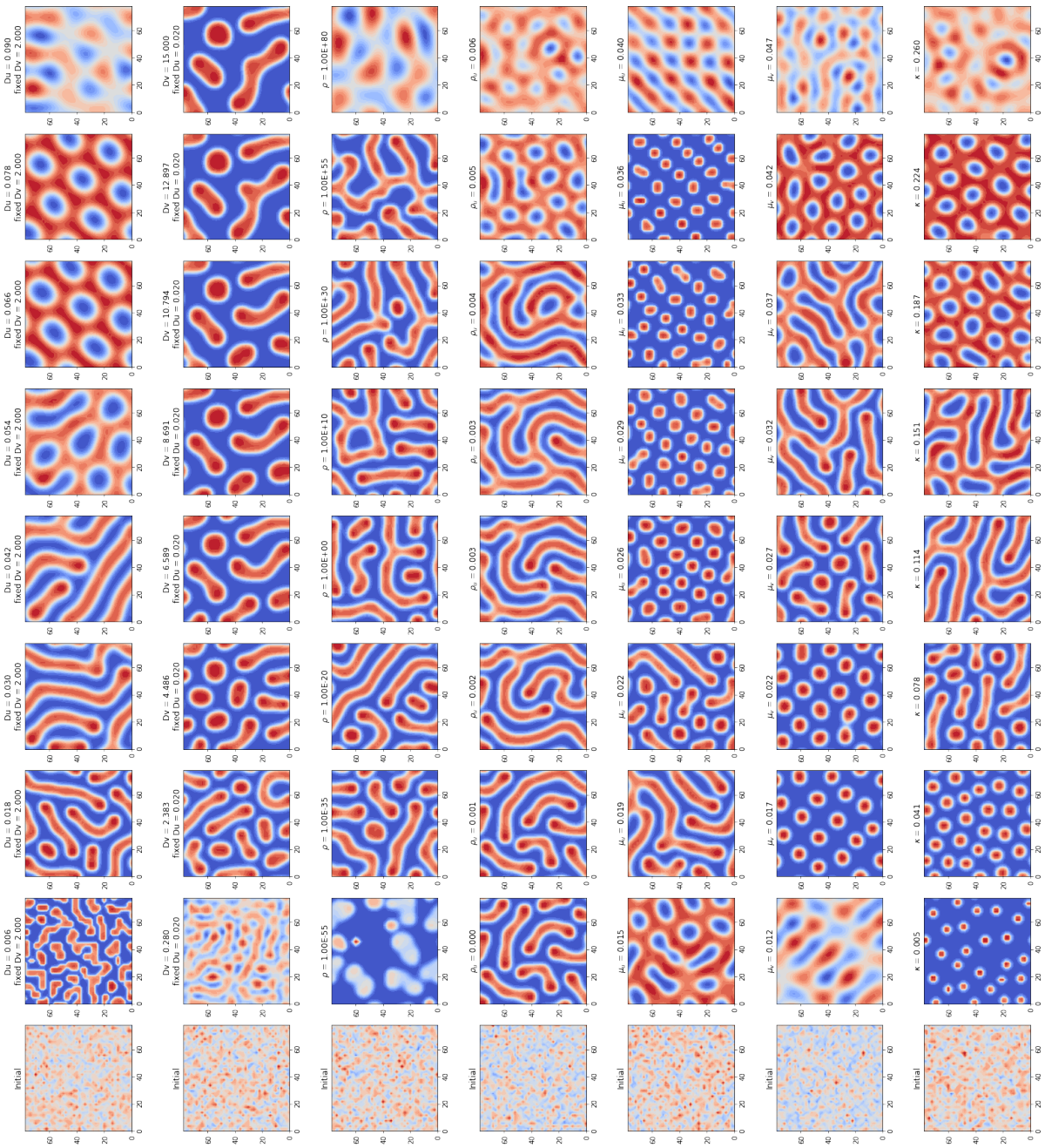

Figure 14: GM: Effects of Parameters

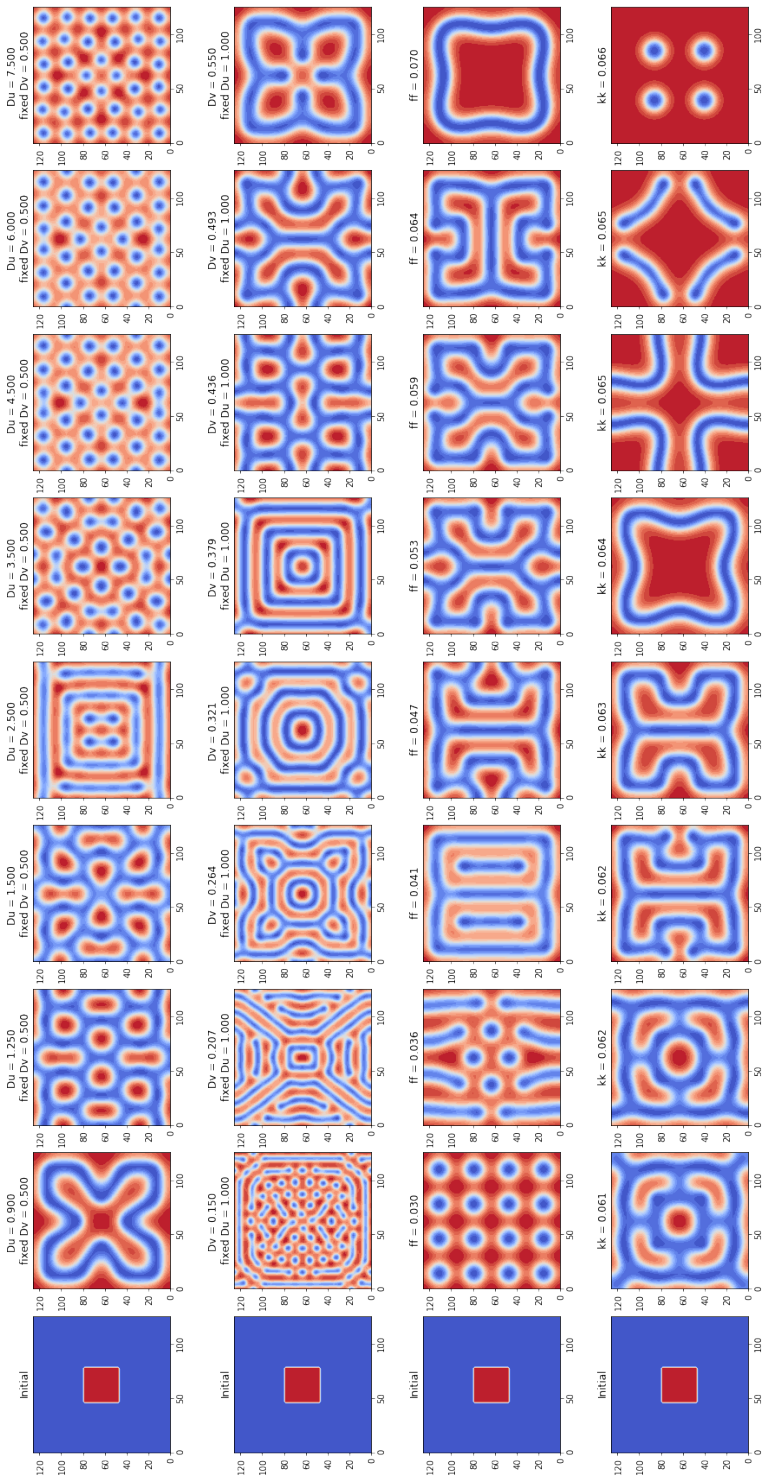

Figure 15: GS: Effects of Parameters

6 Conclusion and Future Work

We aimed to thoroughly study the two representative two-dimensional reaction-diffusion models for pattern formation processes, 1) the Gierer-Meinhardt (GM) model and 2) the Gray-Scott (GS) model. We implemented four numerical methods that varied on the discretization of the diffusion term, forward Euler, backward Euler, Crank-Nicolson, and the ADI method. For each model and each method, we made a series of contour plots of the patterns evolved over time to visualize the pattern's formation process. We used the mean deducted Frobenius norm of the pattern matrix as a quantitative measure of the pattern's salience (contrast).

Comparing the evolution of patterns' and their mean deducted Frobenius norm, we observed that for both GM and GS model, the pattern grows rapidly at first and stabilizes at some time. Comparing the ending state patterns given by each method, the four ending patterns of the GM model agree with each other, while the ending pattern of the GS model given by the ADI method looks different from those given by the other three methods. This is hard to explain because the effects of the nonlinear reaction terms are unclear.

We analyzed the effects of domains, initial conditions, and parameter settings by changing one of these factors at a time while keeping the others fixed. We reproduced results in both the GM and GS model which support Murray's claim that narrow domains only allow bands to grow while wide domain allows stripes or more complicated patterns. We tried four different initial conditions for the GM and the GS model. Though varied initial conditions rendered different patterns, these patterns preserved the symmetry of the initial conditions throughout their formation process. Exploring the parameter spaces of both GM and GS models, we found the range of each parameter for a stable ending pattern.

We envision three directions for future work. First, we applied the periodic boundary conditions in all the numerical algorithms implemented in this project. We may explore other types of boundary conditions (i.e, reflexive boundary condition that the reaction process cannot grow outside the domain; fixed boundary condition that imposes zeros on the boundary). Second, in exploring the parameters' stability range, we only analyzed the effects of changing one parameter at a time while keeping the others fixed. In future work, multiple parameters could be changed together to study their synergetic effect on the pattern formation process. Third, we need additional knowledge of biology in order to better explain the observed effects of changing the domain, initial condition or parameter setting.

7 Acknowledgements

This work is directly inspired by the 2016 Fall AM205 project on modeling shell patterns with RD equations[4]. We really appreciate the help from Luna Lin on the implementation of implicit methods and suggestions for relevant references. We are also grateful to Chris for actively answering our questions throughout the project period.

References

[1] D. R. Fowler, H. Meinhardt, P. Prusinkiewicz, *Modeling seashells*, in: ACM SIGGRAPH Computer Graphics, Vol. 26, ACM, 1992, pp. 379–387.

[2] A. R. Sanderson, R. M. Kirby, C. R. Johnson, L. Yang, *Advanced reaction-diffusion models for texture synthesis*, Journal of graphics tools **11** (3) (2006) 47–71.

[3] J. D. Murray, *How the leopard gets its spots*, Scientific American **258** (3) (1988) 80–87.

[4] H. Meinhardt, M. Klingler, *A model for pattern formation on the shells of molluscs*, Journal of Theoretical Biology **126** (1) (1987) 63–89.

[5] A. Gierer, H. Meinhardt, *A theory of biological pattern formation*, Biological Cybernetics **12** (1) (1972) 30–39.

[6] J. E. Pearson, *Complex patterns in a simple system*, SCIENCE-NEW YORK THEN WASHINGTON- **261** (1993) 189–189.

[7] J. Douglas, Jr, *On the Numerical Integration of* $\frac{\partial^2 u}{\partial x^2} + \frac{\partial^2 u}{\partial y^2} = \frac{\partial u}{\partial t}$ *by Implicit Methods*, Journal of the society for industrial and applied mathematics **3** (1) (1955) 42–65.

[4] L.Brown, S.Chen, Y.Lin, *Modeling Patterns on Shells of Mollusks with Reaction-Diffusion Equations*, 2016